

# Magnetoresistance and robust resistivity plateau in MoAs<sub>2</sub>

Jialu Wang<sup>1</sup>, Lin Li<sup>1</sup>, Wei You<sup>1</sup>, Tingting Wang<sup>1</sup>, Chao Cao<sup>1</sup>, Jianhui Dai<sup>\*,1</sup>, Yuke Li<sup>\*,1</sup>  
<sup>1</sup>*Department of Physics and Hangzhou Key Laboratory of Quantum Matters,  
Hangzhou Normal University, Hangzhou 310036, China*

We have grown the MoAs<sub>2</sub> single crystal which crystallizes in a monoclinic structure with  $C_{12/m1}$  space group. Transport measurements show that MoAs<sub>2</sub> displays a metallic behavior at zero field and undergoes a metal-to-semiconductor crossover below 70 K when the applied magnetic field is over 5 T. A robust resistivity plateau appears below 18 K and persists for the field up to 9 T. A large positive magnetoresistance, reaching about 2600% at 2 K and 9 T, is observed when the field is perpendicular to the current direction. The magnetoresistance becomes negative below 40 K when the field is parallel to the current direction. The Hall resistivity shows the non-linear field-dependence below 100 K. All these results enrich the transport properties of the transition-metal dipnictides, a large family which in general displays variable metallic and topological features.

Three-dimensional(3D) topological quantum materials, including topological insulators (TIs)<sup>1</sup>, topological Dirac semimetals (DSMs)<sup>2–6</sup> and Weyl semimetals (WSMs)<sup>7–14</sup>, have been discovered and intensively investigated recently. These materials exhibit a variety of interesting physical properties, owing to their unique electronic structures and spin textures, and thus show a broad application potential. In an ideal 3D TI where the bulk states are completely gapped out near the Fermi level, a resistivity plateau can clearly develop in the low temperature regime because the only participating surface states are robust to disorders as protected by time-reversal symmetry (TRS)<sup>15–18</sup>. In an ideal WSM, the Weyl fermions disperse linearly all the way across the Weyl nodes which appear in pairs with opposite chiralities by breaking TRS or inversion symmetry<sup>19–21</sup>. The relativistic electronic dispersion and chirality-based topological property result in various semi-metallic transport properties and produce a number of novel phenomena such as the anomalous Hall effect<sup>7</sup> and the Fermi arcs<sup>9</sup>.

Recently, the WSMs have been theoretically predicted and experimentally discovered in a family of transition-metal pnictides represented by TaAs compound<sup>7–14,21</sup>. Consequently, dozens of topological semimetals showing exotic physical properties were reported and studied in detail, such as ZrSiS(Te)<sup>22,23</sup>, MoTe<sub>2</sub><sup>24,25</sup> and LaSb<sup>26</sup>, in addition to the TaAs family. All these materials are non-centrosymmetric in the crystal structure and are further classified into two types of Weyl fermions: with or without the Lorentz symmetry in their energy-momentum dispersions. More recently, a new family of topological semimetals (TSMs) which crystallize in the centrosymmetry monoclinic structure, the transition-metal dipnictides  $XPn_2$  ( $X=\text{Ta, Nb}$ ,  $Pn=\text{P, As, Sb}$ ) as represented by TaSb<sub>2</sub>, have been discovered<sup>27–33</sup>.

The electronic structures of this family involve both disentangled bulk electron/hole bands crossing the Fermi level and topological non-trivial surface states<sup>34</sup>. As a result, they exhibit the extremely large magnetoresistance (MR) and ultrahigh electronic mobility in common, in addition to the low-temperature resistivity plateau and negative MR which are variable across the family. All

these properties make this family appealing in fundamental physics and preferable for materials application.

In this paper, we report the discovery of a new member of this family, MoAs<sub>2</sub>, which also crystallizes in a monoclinic structure. Our experimental results indicate that MoAs<sub>2</sub> is more metallic than TaSb<sub>2</sub> or other members in this family, and undergoes a metal-to-semiconductor crossover under the applied magnetic field up to 5 T. In particular, a very clear resistivity plateau is observed below 18 K even in the absence of the magnetic field. The plateau feature is robust against the applied magnetic field up to 9 T. The MR is relatively large for the perpendicular applied field and current, reaching about 2600% at 2 K and 9 T. When the applied field is rotated from perpendicular to parallel to the current direction, the MR drops rapidly and finally becomes negative. The Hall resistivity shows the non-linear field-dependence below 100 K with a sign change indicative of the multiband features.

Very high quality single crystals of monoclinic MoAs<sub>2</sub> were grown through chemical vapor transport reaction using iodine as transport agent. The detailed synthesis procedures can be found in our previous report<sup>27</sup>. X-ray diffraction patterns were obtained using a D/Max-rA diffractometer with CuK<sub>α</sub> radiation and a graphite monochromator at the room temperature. The single crystal X-ray diffraction determines the crystal grown orientation. The composition of the crystals were obtained by energy dispersive X-ray (EDX) spectroscopy. No iodine impurity can be detected in these single crystals. The (magneto)resistivity and Hall coefficient measurements were performed using the standard four-terminal method covering temperatures range from 2 to 300 K in a commercial Quantum Design PPMS-9 system with a torque insert.

Fig. 1 shows the crystal structure, the XRD patterns and the EDX spectroscopy of MoAs<sub>2</sub>. In Fig.1a, MoAs<sub>2</sub> crystallizes in a monoclinic structure with  $C_{12/m1}$  space group, which is common to the  $XPn_2$  family. Fig. 2b displays the single crystal X-ray diffraction of the MoAs<sub>2</sub>, implying that the crystal surface is normal to the c-axis. The b-axis is perpendicular to the ac-plane, and parallel

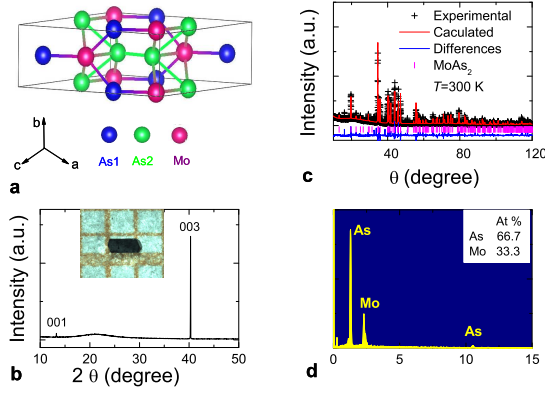


FIG. 1. (a) The crystal structure of  $\text{MoAs}_2$ . (b) Single crystal X-ray diffraction patterns. Inset: picture of a typical  $\text{MoAs}_2$  single crystal. (c) The Rietveld refinement profile for  $\text{MoAs}_2$  sample at room temperature. (d) EDX spectroscopy of spectroscopy at room temperature.

to the current direction. The inset of Fig. 2b shows a picture of a large polyhedral  $\text{MoAs}_2$  crystal with millimeter dimension. The polyhedral crystal with rectangle-shape is consistent with the monoclinic structure. Fig. 1c exhibits the Rietveld refinement profile and its structure parameters in  $\text{MoAs}_2$  at room temperature. The lattice parameters are  $a = 9.064(7)$  Å,  $b = 3.987(1)$  Å,  $c = 7.7182(9)$  Å, and  $\beta = 119.37(1)^\circ$  by the Rietveld structural refinement. Fig. 1d shows the EDX data with the Mo and As contents of 33.3% and 66.7%, respectively, consistent with the ratio of Mo and As.

Figure 2 displays the evolution of the magneto-resistivity as a function of temperature in  $\text{MoAs}_2$  down to 2 K, with the applied magnetic field  $\mathbf{B}/c \perp \mathbf{I}$ . As shown in Fig. 2a, the zero field resistivity  $\rho$  exhibits highly metallic behavior. Upon decreasing temperature, it decreases almost linearly in the high temperature regime until 100 K, below which it shows the Fermi liquid behavior following  $\rho = \rho_0 + AT^2$ . Below 30 K, however,  $\rho$  deviates from the Fermi liquid behavior and remains almost constant, displaying a resistivity plateau as shown in the inset of Fig. 2a. The value of  $\rho$  at 300 K is about  $163 \mu\Omega \text{ cm}$ , comparable to that of high quality  $\text{WTe}_2$ <sup>35</sup> and  $\text{MoTe}_2$ <sup>24</sup>, the potential candidates of the type-II WSM. While,  $\rho$  at 2 K falls to  $0.29 \mu\Omega \text{ cm}$ , yielding a large value of  $\text{RRR}=562$ . This confirms the high quality of the crystal. The extraordinarily low residual resistivity at 2 K was previously found in  $\text{Cd}_3\text{As}_2$ <sup>36</sup>,  $\text{LaSb}$ <sup>26</sup>,  $\text{ZrSiS}$ <sup>37</sup> and high purity  $\text{Bi}$ <sup>38</sup> with very large RRR.

When a magnetic field is applied, the resistivity keeps almost unchanged in the high temperature regime as compared with that of the zero field. A significant change in  $\rho$  appears around 40 K, where the resistivity starts to saturate for small field or crossovers to the semiconductor behavior for large field. After the crossover the resistivity is soon saturated, developing a robust resistivity plateau in the low temperature regime below 18 K as clearly ob-

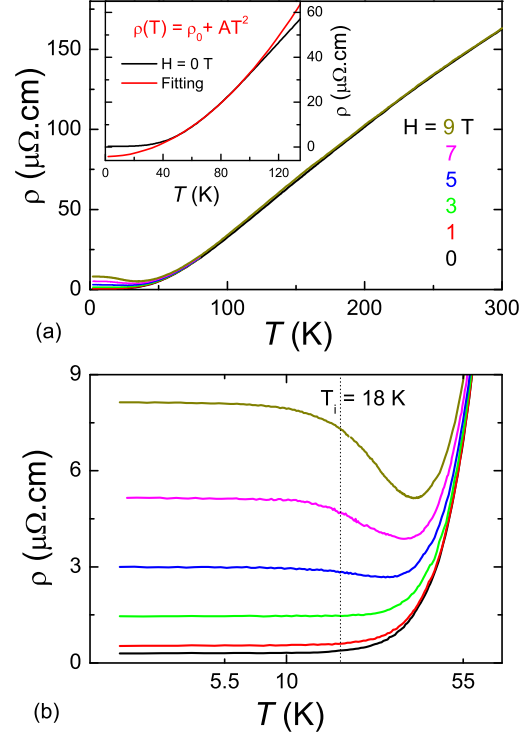


FIG. 2. **Temperature dependence of resistivity for  $\text{MoAs}_2$ .** **a**, Resistivity of  $\text{MoAs}_2$  as a function of temperature in several magnetic fields ( $B = 1, 3, 5, 7, 9$  T.) perpendicular to the current. Inset shows a deviated Fermi liquid behavior below 30 K at  $B = 0$ . The **b** shows a clear plateau resistivity at low temperature.

served in the Fig. 2b. The crossover behavior becomes prominent with increasing magnetic field up to 9 T while the crossover temperature does not change too much.

Similar metal-to-semiconductor/insulator crossovers or transitions were observed in many semimetallic compounds possessing low carrier density and high mobility. In these compounds, saturated resistivity plateaus at much lower temperatures are naturally expected. The microscopic origin of this phenomenon remains debated, depending on the expanded energy scale around which the plateau feature sets in. In the candidates of TIs,  $\text{SmB}_6$ <sup>17,18</sup> and  $\text{LaSb}$ <sup>26,39</sup>, the resistivity plateau is well-attributed to the topological non-trivial surface states which are robust against disorders. It is interesting that a clear resistivity plateau was also observed in  $\text{TaSb}_2$ , a candidate of TSM<sup>27</sup>. Although bulk excitations are involved in this material, the resistivity plateau is plausibly due to the surface states which are topological non-trivial in the sense of doped weak TIs<sup>34</sup>. It is remarkable that the resistivity plateau of  $\text{MoAs}_2$  sets in at  $T = 18$  K, about four times of that of  $\text{SmB}_6$  ( $T = 5$  K)<sup>18</sup>. To the best of our knowledge, this is the highest temperature scale for the emergent resistivity plateau among the topological materials.

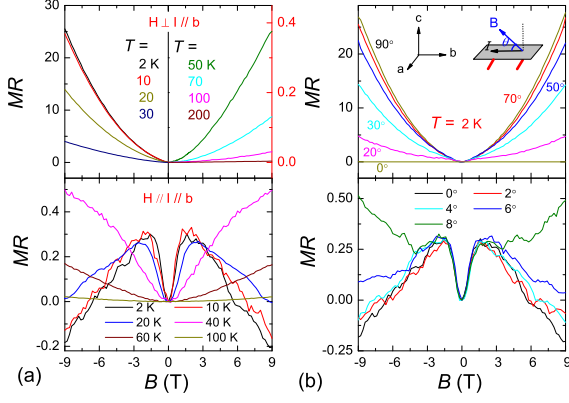


FIG. 3. **Magnetic field dependence of MR in MoAs<sub>2</sub> single crystal.** **a**, the upper panel: Magnetoresistance ( $MR = (\rho_{xx}(H) - \rho_{xx}(0))/\rho_{xx}(0)$ ) versus magnetic fields along the  $c$ -axis at different temperatures as  $\mathbf{B} \perp \mathbf{I} \parallel \mathbf{b}$ . The low panel: MR vs. fields for  $\mathbf{B} \parallel \mathbf{I} \parallel \mathbf{b}$ . **b**, The upper panel: MR plotted as a function of magnetic fields at different angles between  $\mathbf{B}$  and  $\mathbf{I}$ . The low panel: the large and unsaturated negative MR emerges in a narrow window of angle around  $\theta = 0^\circ$ .

Now we turn to the MR of MoAs<sub>2</sub>, defined as  $MR = (\rho(B) - \rho(0))/\rho(0)$ , as shown in Figure 3. All data here are displayed without a symmetrizing process. In the upper panel of Figure 3a, a large MR at low temperatures is observed when the field is perpendicular to the current direction. The MR reaches about 2600% at 2 K and 9 T. The value of MR does not change significantly until 20 K where it decreases sharply in consistent with the robust resistivity plateau which persists up to 9 T. At fixed temperatures, the MR increases quadratically for low field and almost linear for larger field without saturation, similar to the previously-known semimetallic materials including TaAs(P)<sup>7,14</sup>, NbAs(P)<sup>7,14</sup> and WTe<sub>2</sub><sup>35</sup>. Further increasing temperature, its value approaches to 3% at 100K, and is less than 1% above 200 K at 9 T. This feature is in contrast to most of semimetals where a relatively large MR is observed even at the room temperature<sup>14,22</sup>.

As the magnetic field is applied along the current direction,  $\mathbf{B} \parallel \mathbf{I}$ , the MR becomes negative at low temperatures as shown in the low panel of Figure 2a. These MR curves are overall axial-symmetric around  $B = 0$  T, with only slight noises due to the extraordinarily low resistivity. The absolute value of MR is much smaller than that in the case of  $\mathbf{B} \perp \mathbf{I}$ . At 2 K, the MR first increases until about 2 T, then decreases monotonously with the field and changes a sign from positive to negative as  $B \lesssim 6.5$  T, reaching about 20% at 9 T. The negative MR decreases gradually upon heating and disappears above 40 K, beyond which the MR turns back to positive.

Figure 3b shows the field dependence of MR at various angles  $\theta$  of the magnetic field with respect to the current direction at 2 K. By rotating  $\theta = 90^\circ \rightarrow 0^\circ$ , the MR

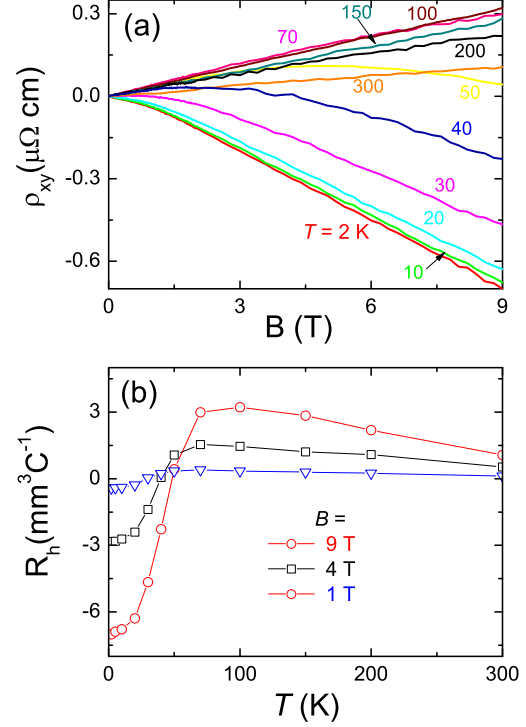


FIG. 4. **Hall effect for MoAs<sub>2</sub>.** **a**, (a) Magnetic field dependence of Hall resistivity at several different temperatures up to 9 T. (b) Hall coefficient vs. temperatures at 1 T, 4 T and 9 T.

drops quickly and shows quadratically field-dependence. The negative MR is further illustrated in the low panel of Figure 3b when  $\theta$  approaches to  $0^\circ$ . At  $B = 9$  T, the MR is still negative for  $\theta \leq 4^\circ$ . When  $\theta$  is larger than  $4^\circ$ , the MR recovers positive and increases with  $\theta$ . The negative MR at  $\theta = 0^\circ$  is limited in a narrow window from this point to  $B \gtrsim 6.5$  T.

The phenomenon of negative MR has been observed in a number of metallic compounds with high mobility of charge carriers. The interpretation of this phenomenon remains debated, too, given the fact that it may appear in both topological trivial and non-trivial materials. A crucial issue behind the negative MR is the current jetting effect due to the field-induced anisotropy. This effect is usually elusive but has been recently suggested as a main cause of negative MR in TaP compound<sup>14,40</sup>. In TaSb<sub>2</sub> compound, however, the current jetting effect was shown to play a minor influence on the negative MR by using different contact configurations<sup>27</sup>. In the ideal WSMs, the negative MR could be best-understood as due to the chiral anomaly. The similar topological interpretation applies to those with ill-defined Weyl points or Dirac points if they appear in pairs and separate in momentum space<sup>41,42</sup>. In the present compound MoAs<sub>2</sub>, the topological interpretation seems consistent with the robust resistivity plateau discussed previously.

Figure 4a maps the magnetic field dependence of the Hall resistivity for MoAs<sub>2</sub> at various temperatures, with the magnetic field ranging from 0 to 9 T. The field dependence of  $\rho_{xy}(B)$  is almost linear with positive slope at high temperature. It starts to bend strongly below 70 K. For  $T \leq 40$  K,  $\rho_{xy}(B)$  shows a pronounced sign reversal from positive to negative, and finally recovers the nearly linear behavior. Fig. 4b shows the temperature dependence of the Hall coefficient at 1 T, 4 T, and 9 T. As temperature decreases,  $R_H$  firstly increases from 300 K, and then undergoes a sharp drop at around 70 K.  $R_H$  changes its sign from positive to negative at around 40 K, implying a partial compensation between the hole-type and electron-type carriers at low temperatures. Using the formula  $n = 1/eR_H(0)$ , where  $R_H(0)$  is the zero temperature limit of  $R_H(B)$ , the electron-type carrier concentration is estimated to be  $n_e = 8 \times 10^{21}$  at 9 T. The calculated carrier mobility is about  $2.69 \times 10^3 \text{ cm}^2 \text{ V}^{-1} \text{ s}^{-1}$  at 2 K. Hence MoAs<sub>2</sub> has a relatively high carrier density of electron-type and a low carrier mobility compared to the typical semimetal compounds<sup>26</sup>.

In summary, we reported the discovery of MoAs<sub>2</sub> compound which crystallizes in the monoclinic structure with a centrosymmetric space group  $C_{12/m1}$ . MoAs<sub>2</sub> undergoes a metal-to-semiconductor crossover below 70 K when the applied magnetic field increases to 5 T. At low temperatures, a clear resistivity plateau with an enhanced temperature scale is observed and this phenomenon is robust against the magnetic field up to

9 T. The compound also exhibits large positive MR and negative MR when the magnetic field is perpendicular and parallel to the current direction, respectively. The robust resistivity plateau, both in the absence and presence of magnetic field, may be due to the topological property of the compound such as the possible topological non-trivial surface states, whose existence should be further examined by experiments and first-principle electronic structure calculations. On the other hand, the Hall resistivity measurement indicates the high carrier density and low mobility in contrast to the most of previously-known topological semimetal materials. Given the excellent metallicity, the robust resistivity plateau, as well as the negative MR, this material adds to the family of the transition-metal dipnictides with potentially preferable applications.

## ACKNOWLEDGMENTS

This research was supported in part by the NSF of China (under Grants No. 11274006 and No. 11274084) and the National Basic Research Program (under Grant No. 2014CB648400). We would like to thank Yi Liu, Jianhua Du and Qunlin Ye for technique assistances. The authors are grateful to Hangdong Wang for stimulating discussions.

- 
- <sup>1</sup> M. Z. Hasan, and C. L. Kane, Rev. Mod. Phys. **82**, 3045 (2010).
  - <sup>2</sup> Z. J. Wang, Y. Sun, X. Q. Chen, C. Franchini, G. Xu, H. Weng, X. Dai, and Z. Fang, Phys. Rev. B **85**, 195320 (2012).
  - <sup>3</sup> S. M. Young, S. Zaheer, J. C. Y. Teo, C. L. Kane, E. J. Mele, and A. M. Rappe, Phys. Rev. Lett. **108**, 140405 (2012).
  - <sup>4</sup> Z. K. Liu, B. Zhou, Y. Zhang, Z. J. Wang, H. M. Weng, D. Prabhakaran, S. K. Mo, Z. X. Shen, Z. Fang, X. Dai, Z. Hussain, Y. L. Chen, Science **343**, 864 (2014).
  - <sup>5</sup> S. Jeon, B. B. Zhou, A. Gyenis, B. E. Feldman, I. Kimchi, A. C. Potter, Q. D. Gibson, R. J. Cava, A. Vishwanath and A. Yazdani, Nature Mater. **13**, 851 (2014).
  - <sup>6</sup> M. Neupane, S. Y. Xu, R. Sankar, N. Alidoust, G. Bian, C. Liu, I. Belopolski, T. R. Chang, H. T. Jeng, H. Lin, A. Bansil, F. Chou and M. Z. Hasan, Nat. Commun. **5**, 3786 (2014).
  - <sup>7</sup> S. M. Huang, S. Y. Xu, I. Belopolski, C. C. Lee, G. Chang, B. Wang, N. Alidoust, G. Bian, M. Neupane, C. Zhang, S. Jia, A. Bansil, H. Lin, and M. Z. Hasan, Nature Commun. **6**, 7373 (2015).
  - <sup>8</sup> C. Zhang, Z. Yuan, S. Xu, Z. Lin, B. Tong, M. Z. Hasan, J. Wang, C. Zhang, and S. Jia, arXiv: 1502.00251 (2015).
  - <sup>9</sup> S. Y. Xu, I. Belopolski, N. Alidoust, M. Neupane, G. Bian, C. Zhang, R. Sankar, G. Chang, Z. Yuan, C. C. Lee, S.-M. Huang, H. Zheng, J. Ma, D. S. Sanchez, B. Wang, A. Bansil, F. Chou, P. P. Shibayev, H. Lin, S. Jia, and M. Z. Hasan, Science **349**, 613 (2015).
  - <sup>10</sup> B.Q. Lv, H. M. Weng, B. B. Fu, X. P. Wang, H. Miao, J. Ma, P. Richard, X. C. Huang, L. X. Zhao, G. F. Chen, Z. Fang, X. Dai, T. Qian, and H. Ding, Phys. Rev. X **5**, 031013 (2015).
  - <sup>11</sup> N. J. Ghimire, Y. Luo, M. Neupane, D. J. Williams, E. D. Bauer, and F. Ronning, J. Phys.: Condens. Matter **27**, 152201 (2015).
  - <sup>12</sup> S.-Y. Xu, N. Alidoust, I. Belopolski, Z. Yuan, G. Bian, T.-R. Chang, H. Zheng, V. N. Strocov, D. S. Sanchez, G. Chang, C. Zhang, D. Mou, Y. Wu, L. Huang, C.-C. Lee, S.-M. Huang, B. Wang, A. Bansil, H.-T. Jeng, T. Neupert, A. Kaminski, H. Lin, S. Jia, and M. Z. Hasan, Nat. Phys. **11**, 748 (2015).
  - <sup>13</sup> C. Shekhar, A. K. Nayak, Y. Sun, M. Schmidt, M. Nicklas, I. Leermakers, U. Zeitler, Y. Skourski, J. Wosnitza, Z. Liu, Y. Chen, W. Schnelle, H. Borrmann, Y. Grin, C. Felser, and B. Yan, Nat. Phys. **11**, 645 (2015).
  - <sup>14</sup> F. Arnold, C. Shekhar, S.-C. Wu, Y. Sun, R. D. d. Reis, N. Kumar, M. Naumann, M. O. Ajeesh, M. Schmidt, A. G. Grushin, J. H. Bardarson, M. Baenitz, D. Sokolov, H. Borrmann, M. Nicklas, C. Felser, E. Hassinger, and B. Yan, Nat. Commun. **7**, 11615 (2016).
  - <sup>15</sup> Z. Ren, A. A. Taskin, S. Sasaki, K. Segawa, and Y. Ando, Phys. Rev. B **82**, 241306 (2010).
  - <sup>16</sup> S. Jia, H. Beidenkopf, I. Drozdov, M. K. Fuccillo, J. Seo, J. Xiong, N. P. Ong, A. Yazdani, and R. J. Cava, Phys. Rev. B **86**, 165119 (2012).

- <sup>17</sup> S. Wolgast, C. Kurdak, K. Sun, J. W. Allen, D.-J. Kim, and Z. Fisk, *Phys. Rev. B* **88**, 180405 (2013).
- <sup>18</sup> D. J. Kim, S. Thomas, T. Grant, J. Botimer, Z. Fisk, and J. Xia, *Sci. Rep.* **3**, 3150 (2013).
- <sup>19</sup> X. Wan, A. M. Turner, A. Vishwanath, and S. Y. Savrasov, *Phys. Rev. B* **83**, 205101 (2011).
- <sup>20</sup> G. Xu, H. Weng, Z. Wang, X. Dai, and Z. Fang, *Phys. Rev. Lett.* **107**, 186806 (2011).
- <sup>21</sup> H. Weng, C. Fang, Z. Fang, B. A. Bernevig, and X. Dai, *Phys. Rev. X* **5**, 011029 (2015).
- <sup>22</sup> L. M. Schoop, M. N. Ali, C. Strar, V. Duppel, S. S. P. Parkin, B. V. Lotsch, and C. R. Ast, *Nature Communications* **7**, 11696 (2016).
- <sup>23</sup> J. Hu, Z. Tang, J. Liu, X. Liu, Y. Zhu, D. Graf, Y. Shi, S. Che, C. Lau, J. Wei, Z. Mao, *Phys. Rev. Lett.* **117**, 016602 (2016).
- <sup>24</sup> Y. Sun, S. C. Wu, M. N. Ali, C. Felser, B. H. Yan, *Phys. Rev. B* **92**, 161107 (2015).
- <sup>25</sup> Z. J. Wang, D. Gresch, A. A. Soluyanov, W. Xie, S. Kushwaha, X. Dai, M. Troyer, R. J. Cava, B. A. Bernevig, *Phys. Rev. Lett.* **117**, 056805 (2016).
- <sup>26</sup> F. F. Tafti, Q. D. Gibson, S. K. Kushwaha, N. Haldolaarachchige, and R. J. Cava, *Nat. Phys.* **12**, 272 (2016).
- <sup>27</sup> Y. K. Li, L. Li, J. Wang, T. Wang, X. Xu, C. Xi, C. Cao, and J. Dai, *Phys. Rev. B* **94**, 121115 (2016).
- <sup>28</sup> Y. Y. Wang, Q. H. Yu, and T. L. Xia, *Phys. Rev. B* **94**, 041103 (2016).
- <sup>29</sup> D. S. Wu, J. Liao, W. Yi, X. Wang, P. Li, H. Weng, Y. G. Shi, Y. Li, J. Luo, X. Dai, Z. Fang, *Appl. Phys. Lett.*, **108**, 042105 (2016).
- <sup>30</sup> Y. K. Luo, R. D. McDonald, P. F. S. Rosa, B. Scott, N. Wakeham, N. J. Ghimire, E. D. Bauer, J. D. Thompson, F. Ronning, *Sci. Rep.* **6**, 27294 (2016).
- <sup>31</sup> Z. J. Yuan, H. Lu, Y. Liu, J. Wang, S. Jia, *Phys. Rev. B* **93**, 184405 (2016).
- <sup>32</sup> B. Shen, X. Y. Deng, G. Kotliar, N. Ni, *Phys. Rev. B* **93**, 195119 (2016).
- <sup>33</sup> Y. P. Li, Z. Wang, Y. Lu, X. Yang, Z. Shen, F. Sheng, C. u Feng, Y. Zheng, Z. A. Xu, arXiv:1603.04056
- <sup>34</sup> C. Cu, J. Chen, G.-X. Zhi, Y. Li, J. Dai, and C. Cao, *Phys. Rev. B* **93**, 195106 (2016).
- <sup>35</sup> M. N. Ali, J. Xiong, S. Flynn, J. Tao, Q. D. Gibson, L. M. Schoop, T. Liang, N. Haldolaarachchige, M. Hirschberger, N. P. Ong, and R. J. Cava, *Nature* **514**, 205 (2014).
- <sup>36</sup> T. Liang, Q. Gibson, M. N. Ali, M. Liu, R. Cava, and N. Ong, *Nature Materials* **14**, 280 (2014).
- <sup>37</sup> M. N. Ali, L. M. Schoop, C. Garg, J. M. Lippmann, E. Lara, B. Lotsch, S. Parkin, arXiv: 1603.09318 (2016).
- <sup>38</sup> P. B. Alers and R. T. Webber, *Phys. Rev.* **91**, 1060 (1953).
- <sup>39</sup> M. Zeng, C. Fang, G. Chang, Y.-A. Chen, T. Hsieh, A. Bansil, H. Lin, and L. Fu, arXiv: 1504.03492 (2015).
- <sup>40</sup> R. D. dos. Reis, M. O. Ajeesh, N. Kumar, F. Arnold, C. Shekhar, M. Naumann, M. Schmidt, M. Nicklas, and E. Hassinger, *New J. Phys.* **18**, 085006 (2016).
- <sup>41</sup> M.C. Chang and M.F. Yang, *Phys. Rev. B* **92**, 205201 (2015);
- <sup>42</sup> J. Ma and D. Pesin, *Phys. Rev. B* **92**, 235205 (2015)